Article

Current Biology

Modulation of Flight Muscle Recruitment and Wing Rotation Enables Hummingbirds to Mitigate Aerial Roll Perturbations

Highlights

- Hummingbirds counter a challenging, continuous perturbation in their first attempt
- Roll control uses bilaterally different muscle activation, posture, and tail fanning
- Differential wing rotation and elevation generate oval versus figure 8 tip trajectories
- Computational simulations show wing rotation to be critical to mitigate perturbation

Authors

Sridhar Ravi, Ryusuke Noda, Susie Gagliardi, ..., Hao Liu, Andrew A. Biewener, Nicolai Konow

Correspondence

nicolai_konow@uml.edu

In Brief

Ravi et al. use a steady longitudinal vortex to determine how fliers counter roll perturbations. Hummingbirds combine bilateral differences in wing elevation and rotation with subtle changes in posture and neuromotor modulation for an elegantly simple yet efficient countering of an unnatural and challenging perturbation.

Ravi et al., 2020, Current Biology *30*, 187–195
January 20, 2020
https://doi.org/10.1016/j.cub.2019.11.025

CellPress

Current Biology
Article

Modulation of Flight Muscle Recruitment and Wing Rotation Enables Hummingbirds to Mitigate Aerial Roll Perturbations

Sridhar Ravi,[1,8] Ryusuke Noda,[2] Susie Gagliardi,[3] Dmitry Kolomenskiy,[4] Stacey Combes,[3] Hao Liu,[5] Andrew A. Biewener,[6] and Nicolai Konow[6,7,8,9,*]
[1]School of Engineering and Information Technology and Australian Defense Force Academy, University of New South Wales, Canberra, Northcott Drive, Campbell, Canberra 2612, Australia
[2]Department of Mechanical Engineering, Kanto Gakuin University, 1 Chome-50-1 Mutsuurahigashi, Kanazawa Ward, Yokohama, Kanagawa 236-8501, Japan
[3]Department of Neurobiology, Physiology and Behavior, University of California, Davis, 155A Hutchison Hall, Davis, CA 95616, USA
[4]Japan Agency for Marine-Earth Science and Technology (JAMSTEC), 2-15, Natsushimacho, Yokosuka, Kanagawa 237-0061, Japan
[5]Graduate School of Engineering, Chiba University, 1-33 Yayoicho, Inage Ward, Chiba 263-8522, Japan
[6]Department of Organismic and Evolutionary Biology, Harvard University, 26 Oxford Street, Cambridge, MA 02138, USA
[7]Department of Biological Sciences, UMass Lowell, Lowell, MA 01854, USA
[8]These authors contributed equally
[9]Lead Contact
*Correspondence: nicolai_konow@uml.edu
https://doi.org/10.1016/j.cub.2019.11.025

SUMMARY

Both biological and artificial fliers must contend with aerial perturbations that are ubiquitous in the outdoor environment. Flapping fliers are generally least stable but also most maneuverable around the roll axis, yet our knowledge of roll control in biological fliers remains limited. Hummingbirds are suitable models for linking aerodynamic perturbations to flight control strategies, as these small, powerful fliers are capable of remaining airborne even in adverse wind conditions. We challenged hummingbirds to fly within a steady, longitudinally (streamwise) oriented vortex that imposed a continuous roll perturbation, measured wing kinematics and neuromotor activation of the flight muscles with synchronized high-speed video and electromyography and used computational fluid dynamics (CFD) to estimate the aerodynamic forces generated by observed wing motions. Hummingbirds responded to the perturbation with bilateral differences in activation of the main flight muscles while maintaining symmetry in most major aspects of wing motion, including stroke amplitude, stroke plane angle, and flapping frequency. Hummingbirds did display consistent bilateral differences in subtler wing kinematic traits, including wing rotation and elevation. CFD modeling revealed that asymmetric wing rotation was critical for attenuating the effects of the perturbation. The birds also augmented flight stabilization by adjusting body and tail posture to expose greater surface area to upwash than to the undesirable downwash. Our results provide insight into the remarkable capacity of hummingbirds to maintain flight control, as well as bio-inspiration for simple yet effective control strategies that could allow robotic fliers to contend with unfamiliar and challenging real-world aerial conditions.

INTRODUCTION

As flying animals navigate their habitats near the Earth's surface, they contend with complex, unpredictable airflows that challenge their aerial stability. To remain airborne, flapping fliers need mechanisms for rapidly adjusting movements with respect to airflow perturbations [1–3]. Whether active or passive in nature, such mechanisms are likely subject to strong natural selection in biological fliers [4] and are critical for sustained flight in artificial fliers [5].

The literature on responses to gust perturbations and chaotic flow in biological fliers is rich. Prior studies have demonstrated the diverse strategies of insects, despite their small size and limited sensorimotor resources, as compared to vertebrate fliers. Passive mechanisms include self-righting through counter-torque produced by flapping [3] and passive inertial control provided by appendages [6]. Insect flight studies also showcase a wide array of active responses, including changes in stroke amplitude [7], angle of attack (AoA) [6, 8, 9], angular rotation [7], and wingbeat frequency [8]. A particularly impressive example is the ability of hawkmoths to negotiate whirlwind perturbations through drastic stroke-to-stroke alterations of wing kinematics [10]. However, it remains largely unknown how vertebrate fliers, such as birds and bats, combine active and passive mechanisms to contend with aerial perturbations.

Compared to insects, vertebrate fliers have more elaborate nervous systems that may confer greater neuromuscular control of their more articulated wing systems. Bats, for instance, harness inertial effects by asymmetrically folding their wings to

perform acrobatic aerial maneuvers [11, 12], which may also contribute to their perturbation responses. Birds have fewer distal wing joints than bats, which reduces their wing kinematic complexity and thus makes birds a more tractable system for understanding vertebrate control responses to aerial perturbations. Hummingbirds, in particular, are well-studied, small, powerful flyers that are highly amenable to wind tunnel experiments. Hummingbird wing kinematics [13] and muscle activity patterns [14, 15] in laminar flow have already been established across a range of forward flight speeds. Previous studies have also shown that hummingbirds can navigate unsteady wakes and turbulent air flow by altering stroke amplitude, frequency, and a range of other wing kinematic parameters [16, 17], as well as fanning their tails to actively maintain flight control [17]. This wealth of background data on hummingbird flight makes them an ideal model system for examining neuromuscular flight control in the face of challenging, aerial perturbations.

Flight control in the face of aerodynamic perturbations involves both passive and active mechanisms [1]. However, it remains unclear exactly how neuromotor control drives active responses to flight perturbations. Neuromotor modulation may be key for shaping both kinematic and behavioral responses to perturbations [14, 18]. Studies of small (mainly invertebrate) fliers have begun to "close the loop" by linking kinematics to neuromotor control [19–21] and (via empirical or computational fluid dynamics [CFD] approaches) to the production of aerodynamic forces, in still air as well as unsteady, perturbed flow [9, 10, 16, 22]. For vertebrate fliers, some studies have begun linking kinematics to motor control [14, 15, 23, 24] and estimating the aerodynamic forces that result via CFD [18, 25] and empirical associations [26]. However, these approaches have yet to be combined for studies of vertebrate fliers subjected to aerodynamic perturbations during flight.

Here, we generated a nominally time-invariant vortex that is oriented longitudinally (with its core oriented streamwise along the axis of the wind tunnel) to impose an extreme and continuous aerodynamic perturbation on flying hummingbirds (*Archilochus colubris*). The positioning of the vortex core relative to a feeder means that birds experience upwash on one wing and downwash on the other, which induces a strong, continuous roll perturbation (Figure 1). Within this challenging yet predictable aerial environment, we analyzed the response of subjects in terms of both wing kinematics and neuromuscular control, using 3D high-speed video to quantify kinematics and electromyography to determine neuromotor modulation of the pectoralis (primary downstroke muscle) and supracoracoideus (primary upstroke muscle) with respect to airflow conditions.

We then use CFD simulations to assess the functional role of observed changes in wing motions. We first assessed the impact of a longitudinal vortex created in the CFD domain, nominally similar to experiment, on a hummingbird flying with steady wing kinematics. However, performing CFD simulations with a longitudinal vortex that matches experimental measurements as well as a flapping bird downstream is currently not feasible. Therefore, we conducted further simulations in steady (laminar) flow using the kinematics measured on birds flying in a longitudinal vortex. We hypothesized that deploying the observed kinematics in laminar flow should result in bilaterally asymmetric lift production and a roll toque in the direction opposite to that imposed on real birds by the vortex flow. The CFD model is also used to perform comparative analysis of the contribution of individual kinematic changes to overall stabilization of the perturbation by modeling different parameters in isolation. This workflow allows us to identify the key response parameters for flight stabilization and disturbance rejection.

Studies of aerial perturbations have historically been focused on yaw and pitch perturbations [6, 27, 28]. However, roll remains a vital maneuvering and stability mode with a smaller moment of inertia than the pitch and yaw axes in many flying animals [29]. Accordingly, we hypothesize that a strong, flow-induced roll torque will elicit bilaterally asymmetric wing kinematics to produce a compensatory counter-torque. However, determining whether observed kinematic changes are entirely passive (i.e., induced by the external flow) or in fact are generated actively by the bird requires direct measurement of the neuromotor response. Previous work has shown that voluntary maneuvering during yaw turns and abrupt course changes in hummingbirds and cockatoos involve no bilateral variation in activation (duration of neural stimulation) or recruitment (measured as electromyogram [EMG] amplitude, a proxy for the number of motor units and volume of muscle activated) of the largest flight muscles (pectoralis and supracoracoideus) [30, 31]. However, as hummingbirds engage in unsteady flight, e.g., during mating displays, they use significant asymmetry in wing kinematics [30, 32, 33] that are associated with variations in the recruitment pattern of major flight muscles and consistent with feedforward control [30].

The upwash produced by our longitudinal vortex should reduce the need for aerodynamic force production by the wing subjected to it. Therefore, we hypothesize that hummingbirds will respond by displaying lower wing-stroke amplitude and/or a longer downstroke duration (i.e., slower velocity) in this wing (kinematic response), driven by decreased muscle activation and recruitment (EMG) of the associated flight muscles (neuromotor response). This combination would be expected to result in reduced aerodynamic force production from this wing, whereas for the wing subjected to the downwash of the longitudinal vortex, we predict increases in the same kinematic and neuromotor parameters to provide increased production of aerodynamic force. The difference in force production between the two wings should result in a stabilizing counter-torque on the body.

RESULTS

Wingbeat Kinematics

Mean wingbeat frequency, stroke amplitude, and stroke-plane angle employed by birds flying in the vortex and laminar flow conditions were statistically indistinguishable (tested for differences between wings within each flow treatment, as well as across the different flow conditions, with ANOVA; all $p > 0.15$; Table S1). There were also no statistically significant differences in mean angular wing position across airflow conditions (Figure 2C). However, during flight in the longitudinal vortex, all four subjects displayed consistent, bilateral differences in wing elevation and rotation patterns. In laminar flow, there was no bilateral asymmetry in the mean or instantaneous angles of wing elevation and rotation, whereas during flight in the longitudinal vortex, the kinematics of a given wing were

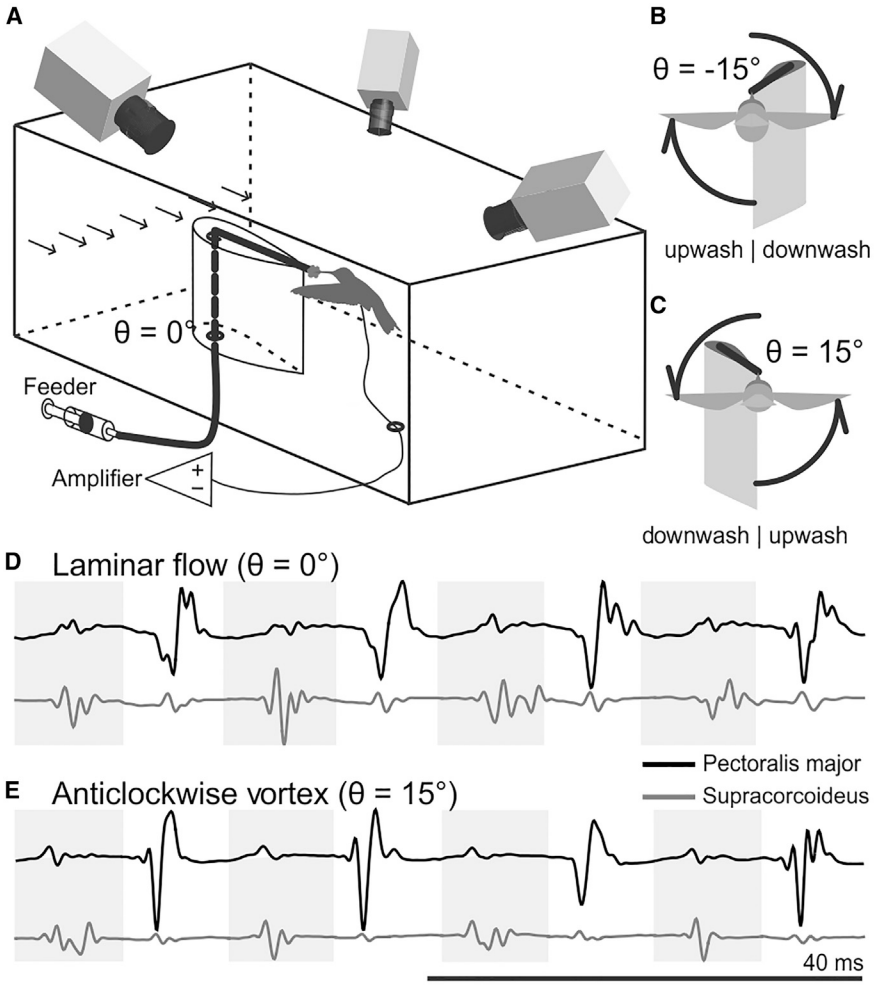

Figure 1. Schematic of Experimental Set-Up for Performing *In Vivo* Measurements of Hummingbird Flight Kinematics and Neuromotor Modulation in a Steady Roll Perturbation

(A) A nectar supply elicited flight in the near wake of a vertically oriented airfoil.

(B and C) With the vortex generator rotated at −15° relative to the oncoming flow, (B) a sustained, longitudinal tip vortex (parallel to streamwise flow within the wind tunnel) generated upwash on the left wing and downwash on the right (see also Figure S1) and (C) a vortex with reverse orientation is created when the vortex generator was positioned at 15° with respect to the oncoming flow.

(D and E) EMGs were recorded from the left pectoralis (red) and supracoracoideus (dark grey) during flight in (D) laminar flow and (E) in longitudinal vortex flow. For (D) and (E), sample EMG data for four wingbeat cycles are shown, and gray shading represents the downstroke.

Sample flight video and EMG recordings are in Video S1.

strongly dependent on the local airflow condition (either upwash or downwash; Figures 2D and 2E). Due to asymmetries in wing elevation patterns between the two wings, the path of the leading edge of the wing resembled a figure eight pattern when in the upwash but an oval path when in the downwash of the longitudinal vortex (Figures 2F–2H). Except for early in the downstroke, when wing rotation was similar among all three flow conditions, overall wing rotation was greater for the wing in upwash than for the wing in downwash (Figures 2E–2H). The birds maintained these asymmetries in wing kinematics throughout the entire duration (5- to 10-s feeding bouts) of their flight in the longitudinal vortex flow. At 75% span, the wing in the vortex downwash operated at higher AoA (Figure S3) during the downstroke as compared to the wing in laminar and vortex upwash conditions. At the same spanwise location, during upstroke, nominally similar AoA was noted for both downwash and laminar flow conditions, although AoA was lower for the wing in the upwash (Figure S4).

No significant differences were observed in mean body roll or pitch angle for any of the flight conditions. However, the mean yaw angle of the body differed significantly between laminar flow and clockwise versus counterclockwise vortex conditions ($F_{2,16} = 4.51$; $p < 0.001$; Figure 3A). In steady, laminar wind, the birds were aligned with the longitudinal axis of the wind tunnel, but when confronted with the clockwise vortex, they yawed negatively (to their right), and this pattern reversed when they flew in the counterclockwise vortex condition (see Figure 3 for illustration). In addition, tail fan angle during flight in the vortex was greater than during flight in laminar flow flight for all birds ($F_{2,16} = 5.51$; $p < 0.0001$; Figure 3B).

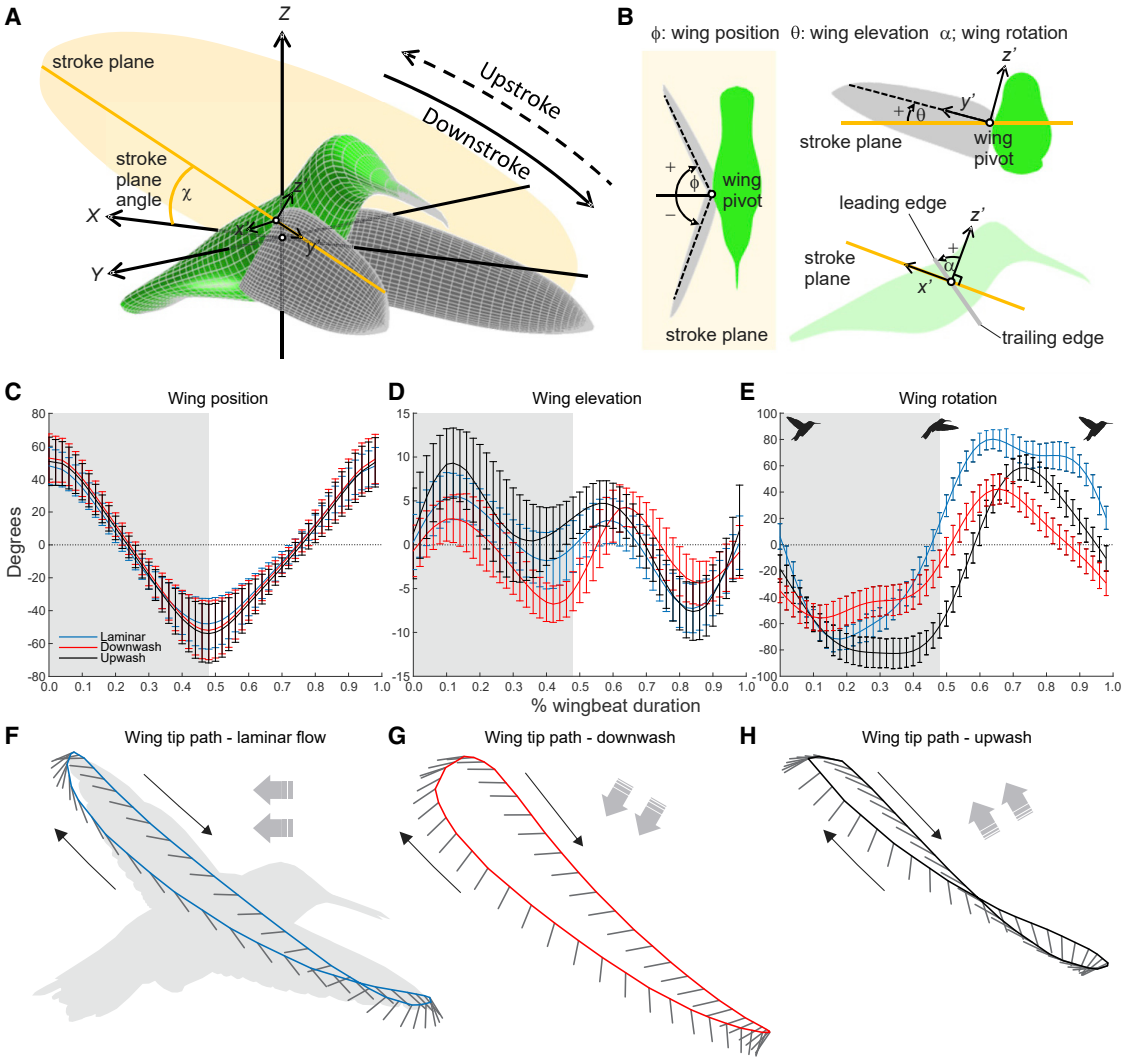

Figure 2. Schematic Defining the Hummingbird Model and Wing Kinematics Results

(A) Hummingbird model with the global coordinate system (*X*, *Y*, *Z*), the wing-fixed coordinate system (*x*', *y*', *z*'), and the stroke plane angle χ.

(B) Wing kinematic parameters with respect to the stroke plane angle: the positional angle Φ; the elevation angle θ; and the rotation angle α.

(C–E) Instantaneous wing position, elevation, and rotation angles measured for the wingtips differed across laminar flow, upwash, and downwash conditions, respectively (gray shading represents downstroke) from 84 wingbeats. Data are means ± 1 SD, with all wingbeats and birds pooled.

(F–H) Sagittal motions of the wing-tip paths for wings differed across the three different flow conditions. Black whiskers represent wing position and cord rotation at successive instances of the wingbeat. Thin black arrows indicate wingtip motion, and gray arrows indicate incident airflow on the wing.

See also Figure S3 for angle of attack at different positions in the wing stroke for the three inflow conditions. Other kinematic and morphological parameters are presented in Tables S1 and S2, respectively.

See also Videos S1 and S2.

Identification of Critical Wing Kinematic Traits

CFD simulation of the hummingbird flying with symmetric kinematics in the relatively mild vortex created by the upstream vortex generator (case 0; Figure S4) indeed caused a large roll torque on the bird (Table 1) that would require compensation. Simulation under laminar conditions of the numerical hummingbird with wing kinematics measured in laminar flow (case 1) resulted in the generation of adequate vertical aerodynamic force to establish weight support (Figures 4A and 4D; Video S2A; Table 1). Weight support was also demonstrated in the simulation using the wing kinematics measured on birds flying in the clockwise vortex, but because the kinematics were tested with laminar inflow in the simulation, they produced a lift imbalance between the wings (case 2; see Figures 4B and 4D; Video S2B; Table 1). The kinematics measured from the wing immersed in downwash produced higher lift compared to the kinematics of the wing in upwash, creating a strong, counterclockwise roll torque, as expected (Table 1; see velocity contours in Figure 4). The torques measured in the CFD simulation are a representation of those produced by the birds when flying in the vortex; in the longitudinal vortex flow experienced by the real birds, this roll torque induced by asymmetric wing kinematics would counteract the torque induced by external flow.

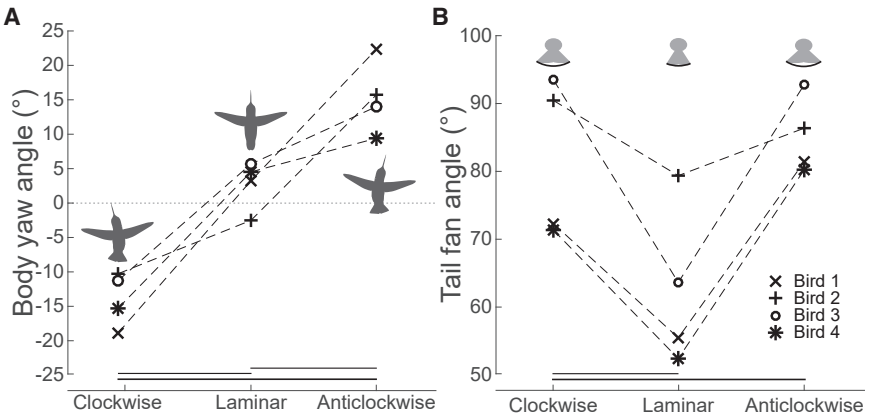

Figure 3. Hummingbird Body and Tail Responses to the Roll Perturbation

Mean angles of (A) body yaw and (B) tail fanning across free-stream conditions. Lines below the data indicate statistically significant ANOVA results (see text for details). See Table S2 for morphological parameters of the birds.

CFD simulations of birds flying with kinematics that were a hybrid between those measured in laminar flow and in the vortex condition allowed us to comparatively assess the significance of each kinematic parameter that differed between the wings during the perturbation response. These simulations revealed that employing bilateral asymmetry in wing rotation angles (matching those measured in the vortex condition) while all other parameters were symmetric (as in the laminar flow condition) produced a vertical force similar to that in laminar flow and approximately 80% of the roll torque produced by fully asymmetric kinematics (cases 2 and 4; Table 1). This roll torque was a result of the wing rotation angle in downwash producing higher lift, and the resulting flow field closely resembled that of experimentally measured kinematics (compare Figures 4B and 4D; Video S2). Simulation of hybrid kinematics involving bilateral asymmetry in the angle of wing elevation alone (case 3) produced a roll torque in the opposite direction of that produced by the fully asymmetric kinematics measured from the hummingbirds (cases 2 and 4; Table 1).

Neuromuscular Activation

Consistent with prior EMG recordings of hummingbird flight muscles [14, 33], activation of the pectoralis occurred during the upstroke and activation of the supracoracoideus occurred during the downstroke. The extreme activation phase advance of these muscles reflects the high wingbeat frequency (~42 Hz) and inherent mechanical delay in force development [18]. Statistical analyses of EMG variables, quantified over each wingbeat, revealed consistent shifts in activation patterns for both muscles. Post hoc tests showed that the pectoralis was activated earlier when the wing was immersed in downwash as compared to upwash conditions (ANOVA; $F_{2,140} = 8.4$; $p < 0.0001$) and that the pectoralis remained active longer in downwash compared to upwash and laminar flow conditions ($F_{2,140} = 14.8$; both $p < 0.001$). The supracoracoideus was also activated earlier and remained active longer when in downwash compared to upwash (onset: ANOVA, $F_{2,140} = 6.1$, $p < 0.01$; duration: $F_{2,140} = 7.8$, $p < 0.0001$; Figure 5A). Normalized mean recruitment intensities (iEMG) of both the pectoralis and supracoracoideus also differed significantly across conditions, with higher iEMG measured when the wing was in downwash as compared to upwash or laminar flow conditions (ANOVA; pectoralis: effect of condition, $F_{2,476} = 34.36$, $p < 0.0001$ for all pairwise comparisons; supracoracoideus: $F_{2,476} = 54.51$, $p < 0.0001$; Figure 5B).

DISCUSSION

Consistent, Sustained Response to a Steady Aerodynamic Disturbance

Here, we subjected hummingbirds to a challenging flow environment: flight within a longitudinal vortex that imposed an extreme, continuous roll perturbation by immersing one wing in upwash and the other in downwash. This environment is unfamiliar to biological fliers and unlikely to occur in nature. Nevertheless, the fact that all subjects produced the corrective forces and torques required to successfully navigate this flow environment on their first attempt attests to the flexibility of hummingbird flight control and offers insight into the primary mechanisms employed to contend with aerodynamically induced roll perturbations.

Table 1. Kinematics Variables Used in the Different Cases for Numerical Simulations and the Mean Vertical Force and Roll Torque Produced

		Wing Kinematics Parameters				
Case	Inflow Condition	Position	Elevation	Rotation	Mean Vertical Force (mN)	Mean Roll Torque, mN · m^{-1}
0	↻	⇆	⇆	⇆	70.1	−408.4
1	⇆	⇆	⇆	⇆	72.7	–
2	⇆	↻	↻	↻	67.2	788.9
3	⇆	⇆	↻	⇆	70.5	−273.0
4	⇆	⇆	⇆	↻	65.2	793.4

Case 0 is a simulation of the hummingbird flying in the longitudinal vortex with kinematics measured in the laminar flow condition; see Figure S4 for flow field comparison and snapshot of simulation. Cases 1 and 2 are simulations of hummingbird flight in steady wind with kinematics measured in the laminar flow condition (1) and in a clockwise vortex (2). Case 3 is a kinematic hybrid between laminar flow and clockwise vortex conditions with wing elevation angles from the clockwise vortex condition and other parameters as measured in laminar flow. Case 4 is another kinematic hybrid with wing elevation and position angles from the laminar flow condition and rotation angles from the clockwise vortex.

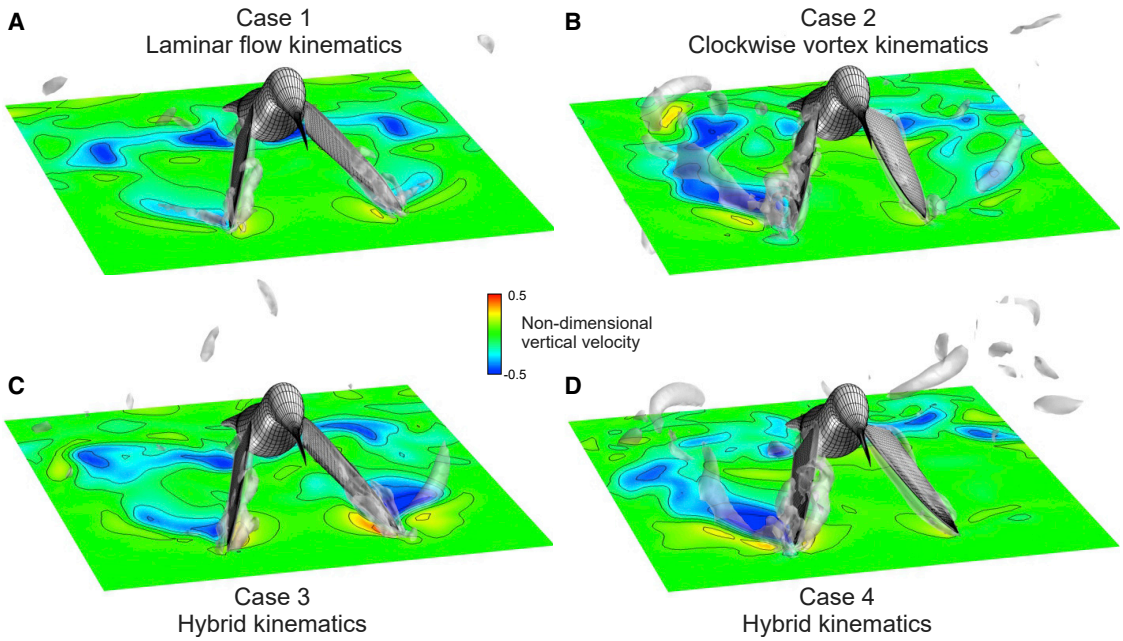

Figure 4. Snapshots of the Flow Fields, at the Bottom of the Downstroke, Derived from Numerical Simulations
Wing kinematics were measured in laminar flow (A) and in the presence of a clockwise, steady roll perturbation (B), as well as hybrid kinematics (C and D) as indicated for cases 1–4 in Table 1. Isosurfaces of dimensionless downward velocity are color coded (note scale bar).
See Figure S2 for information on CFD domain and animation in Video S2.

In laminar flow, hummingbirds displayed wing kinematics that were stable, consistent, and bilaterally symmetric across wingbeats. Traits including stroke plane angle, wingbeat frequency, amplitude, and the time history of wing rotation angles were similar to those reported previously for hummingbirds [14]. In contrast, when hummingbirds flew within the longitudinal vortex, they deployed wing kinematics with bilateral asymmetry in some subtle kinematic variables (Figure 2) to generate the corrective forces and torques that enabled them to successfully attenuate the effects of the perturbation. Bilateral asymmetry in wingbeat kinematics is a common feature in the response arsenal deployed by flying animals in response to aerodynamic disturbances, and our subjects followed this pattern. Asymmetric wing kinematics appear to be a fundamental feature of flight stabilization and maneuvering, used both for dealing with perturbing winds [16, 17] and for engaging in voluntary maneuvers during flight [30]. Although variation in stroke-to-stroke wing kinematics was slightly higher while hummingbirds were flying in the longitudinal vortex as compared to laminar flow (Figures 2C–2E), wing kinematics remained consistent between strokes in the vortex flow and depended primarily on whether the wing was in the upwash or downwash of the vortex. Thus, in the presence of the steady aerodynamic perturbation produced by the longitudinal vortex, the birds produced a consistent, sustained response through systematic changes in subtle features of kinematics. This result contrasts with previous results obtained for hawkmoths (which display similar morphology and kinematics as hummingbirds) when flying within a vertically oriented, steady vortex (i.e., a tornado). Under these conditions, hawkmoths responded with large stroke-to-stroke variation in wing kinematics [10].

Limited Change in Wing Kinematics

Despite the magnitude of the aerodynamic disturbance imposed upon hummingbirds in this study (with one wing completely immersed in upwash and the other in downwash), the bilateral differences observed in wing kinematics were remarkably subtle, and our hypothesis of bilateral asymmetry in stroke amplitude was not supported. Whereas previous studies have shown that many species employ bilateral asymmetries in the overall extent or angle of wing motion (e.g., in stroke amplitude or stroke plane angle) to produce asymmetric forces, the main kinematic variables modulated in hummingbirds while flying in a longitudinal vortex were wing elevation and rotation angles (Figures 2D–2H). During both the upstroke and the downstroke, the wing in upwash was rotated at a steeper angle with respect to the stroke plane, as compared to the wing in upwash (Figure 2E). Therefore, though both wings tended to align with the local airflow, the wing in downwash adopted a greater effective geometric angle (see Figures 2G and 2H) that translated to an increased AoA for the wing in downwash during the powerful downstroke (Figure S4). Operating at higher angles of attack leads to an increase in aerodynamic force [34]. The parametric study conducted using CFD simulations suggests that bilateral asymmetries in wing rotation (as opposed to elevation) were in fact the primary source of the stabilizing roll torques generated by hummingbirds (case 4; Figure 4; Table 1; Video S2).

Other critical kinematic attributes, such as stroke amplitude, stroke plane angle, and flapping frequency, remained unchanged, despite the fact that these parameters play a significant role in force production [34]. Wingbeat amplitude, in particular, is modulated by hummingbirds to adjust power requirements as a function of flight speed [13] and is adjusted

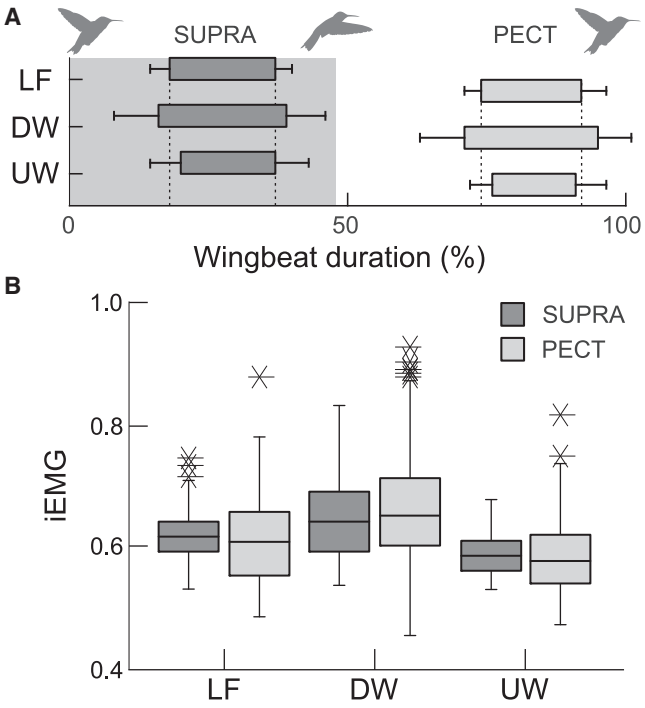

Figure 5. The Neuromuscular Modulation Component of Roll Control

EMG from supracoracoideus (SUPRA) (dark gray) and pectoralis (PECT) (light gray) muscles across flow conditions (DW, downwash; LF, laminar; UW, upwash). Data from all four subjects are pooled for each muscle and condition.

(A) Activation timing. Box bounds show mean timing of EMG onset (left) and offset (right), and whiskers show 1 SD; gray shading indicates downstroke. Mean activation-deactivation timing is prolonged in downwash and truncated in upwash, compared to laminar flow (dashed lines).

(B) Mean recruitment intensity. Box center line is median, bounds are quartiles, and whiskers are 95% ranges.

See text for statistically significant differences.

bilaterally in other flying animals to produce asymmetric forces. Hence, bilateral modulation of this parameter would seem to afford hummingbirds a high level of control authority. Why might hummingbirds abstain from employing these potentially more effective modes of torque generation? One possible explanation is that increases in stroke amplitude and flapping frequency may be energetically more expensive due to the increased drag and inertial costs of changing wing-flapping motions, as compared to the inertial and aerodynamic costs of simply changing wing long-axis rotation. Introducing bilateral asymmetry in the flapping frequency would also likely introduce undesirably large forces and stresses on the thorax. In addition, hummingbirds may favor preserving the capacity to change amplitude and/or frequency (i.e., not exhausting their kinematic response envelope) to allow for sudden responses to threats or greater destabilizing perturbations. Finally, hummingbirds are known to modulate their stroke plane angle depending on their cruising speed [13], and this could explain the lack of difference in stroke plane angle seen here between flight in laminar flow and in the longitudinal vortex (Table S1), because the total oncoming wind speed was similar across different flow conditions.

Muscles Providing Mechanical Power Respond to Wing Loads

While flying in the longitudinal vortex, irrespective of which wing was experiencing upwash or downwash, the coupling between the midpoint of temporal activation of both muscles and stroke phase remained consistent (Figure 5A). However, muscles controlling the wing in downwash, which operates at higher AoA (Figure S4) and likely experiences greater aerodynamic forces, displayed greater levels of motor unit recruitment and were activated over a longer period of time (activated earlier and deactivated later) than muscles controlling the wing in upwash (Figure 5). The wing in upwash was not only able to benefit from the updraft but also needed to produce lower relative force to maintain stable roll orientation of the body. The asymmetry in iEMG of the two main flight muscles likely reflects asymmetries in muscle force production that allow the bird to maintain bilateral *symmetry* in wingbeat frequency and amplitude, despite the vastly different flow environments experienced by the two wings. Thus, bilaterally asymmetric modulation of the activation and recruitment of the large flight muscles was utilized to both produce the necessary aerodynamic forces through wing rotations, likely in combination with smaller distal wing muscles [35], and for producing necessary flight power to support the overall differences in aerodynamic loads acting on the wings.

Central pattern generators (CPGs) are populations of rhythmically active neurons in the brain stem [36]. These neurons are thought to be important neural subsystems for maintaining bilateral control of the timing of muscle activation [37, 38], with important implications for how gait is maintained in limbs and wings during terrestrial and aerial locomotion, respectively [39]. Based on the prominent role of asymmetric wing rotation, with no changes to flapping frequency and phasing, taken together with the inferences from asymmetry in EMG activity, we may postulate that CPG control of the mean timing of activation of the large flight muscles remains largely unchanged, even when confronted with significant aerodynamic perturbations. Meanwhile, smaller intrinsic muscles of the wing may play a critical role in modulating wing forces and body torques. This could potentially be a computationally and energetically effective flight-control strategy as compared to making large-scale changes to muscle recruitment frequency, timing, and magnitude. Indeed, EMG recordings from the pectoralis and supracoracoideus of hummingbirds performing pure yaw maneuvers (no translation) have revealed that, although wing kinematics differed bilaterally and between wingbeats, there was no alteration in the mean timing of activation of the muscles providing flight power [30].

A Mosaic of Active and Passive Mechanisms

Passive interaction between the oncoming airflow and the wings may play a significant and generalizable role in the flight stability of birds in response to unsteady winds. Interactions between the fluid and the active and passive mechanics of the animal have been shown to play an important role in determining locomotion dynamics and control both in aerial and aquatic domains [6, 40]. For the hummingbirds studied here, the observed wing rotations to align with the local airflow in the longitudinal vortex (Figures 2E–2H) may reflect a combination of active control responses and resultant passive aeroelastic interactions. Furthermore, many studies have revealed that wing shape during flapping

can vary along the span and deflection of the feathers can introduce sectional changes resulting in wing twist [41]. Such mechanisms may also influence the wing rotation observed in the hummingbirds here. Because wing rotation was estimated based on motions of the tip of the sixth primary feather on the trailing edge, parameters such as relative feather deflection and wing twist could not be estimated. The role of passive aeroelasticity may be verified by concomitantly performing high-speed videography of the kinematics and measuring the activity of smaller intrinsic wing muscles responsible for kinematic control of wing rotation and shape to determine whether the observed changes in wing rotation were controlled via muscular activation or were the result of passive interactions with the external flow. Obtaining EMG measurements from these smaller muscles, particularly in hummingbirds, and theoretical estimation of passive wing rotation, as performed for insects [2], would be challenging, but this question merits further investigation, perhaps in a larger bird or bat species.

A combination of active behavioral adjustments and passive dynamics may also play a role in flight stabilization, both in terms of the biased yaw angle and the increased tail fanning that hummingbirds deployed in the longitudinal vortex (Figure 3). These postural adjustments could passively augment lift through energy harvesting by increasing the surface area and apportioning a larger part of the thorax and tail over the region of vortex upwash through body yaw (Figure 3). The yaw postural adjustments in the birds may not be entirely active, because the posterior region of the birds remained below the feeder and the longitudinal vortex likely also caused a side force that was oriented toward the region of the upwash. Birds have previously been shown to use tail fanning to increase their longitudinal stability during forward flight, particularly when flying in turbulent winds [16, 17]. When flying in the vortex, hummingbirds could also be actively deploying their tail to overcome forces and torques that may be a consequence of the altered wing kinematics. Hence, it is critical to consider the role of both active and passive interactions with the fluid to understand how biological and artificial flying systems may augment control and alleviate sensorimotor demands for maintaining stable flight in unsteady, unpredictable, and challenging wind conditions.

In conclusion, the postural adjustments, changes in subtle features of wing orientation, and underlying modulation of neuromuscular control that enabled hummingbirds to maintain stable flight with only subtle changes in wing kinematics, in the face of an extremely challenging flow environment, reveal a flight control strategy that is elegant in both its simplicity and efficacy. Such a strategy requires the ability to integrate multiple control subsystems and adeptly modulate localized actuation of the flight system, all being flight control attributes that are exquisitely demonstrated by hummingbirds. Such integrated systems are likely found among other volant vertebrates and provide substrata for bio-inspired development of robust yet responsive control architectures that could be advantageous for robotic flier designs.

STAR★METHODS

Detailed methods are provided in the online version of this paper and include the following:

- KEY RESOURCES TABLE
- LEAD CONTACT AND MATERIALS AVAILABILITY
- EXPERIMENTAL MODEL AND SUBJECT DETAILS
- METHOD DETAILS
  - Electrode implantation for electromyography
  - Flight tests
- QUANTIFICATION AND STATISTICAL ANALYSIS
  - Flow Conditions
  - Reconstruction of kinematics
  - Data analysis and statistical tests
  - Computational fluid dynamics analysis
- DATA AND CODE AVAILABILITY

SUPPLEMENTAL INFORMATION

Supplemental Information can be found online at https://doi.org/10.1016/j.cub.2019.11.025.

ACKNOWLEDGMENTS

The authors would like to thank the four anonymous reviewers for their valuable comments. This work was supported by the Office of Naval Research grant no. N0014-10-1-0951 (A.A.B.), National Science Foundation grant numbers IOS-1253677 and CCF-1253677 (S.C.), Japan Society for the Promotion of Science grant numbers KAKENHI 15F15061 (D.K.) and 24120007 (H.L.), Company of Biologists Traveling Fellowship (S.R.), and start-up funds from UMass Lowell (N.K.).

AUTHOR CONTRIBUTIONS

S.R., N.K., S.G., A.A.B., and S.C. conceptualized and designed the experiments. S.R., N.K., and S.G. performed the experiments, and R.N. and D.K. performed the simulations. All authors contributed in data analysis and writing the manuscript.

DECLARATION OF INTERESTS

The authors declare no competing interests.

Received: May 14, 2019
Revised: October 9, 2019
Accepted: November 7, 2019
Published: January 2, 2020

REFERENCES

1. Dickinson, M.H., Farley, C.T., Full, R.J., Koehl, M.A., Kram, R., and Lehman, S. (2000). How animals move: an integrative view. Science *288*, 100–106.
2. Ristroph, L., Bergou, A.J., Ristroph, G., Coumes, K., Berman, G.J., Guckenheimer, J., Wang, Z.J., and Cohen, I. (2010). Discovering the flight autostabilizer of fruit flies by inducing aerial stumbles. Proc. Natl. Acad. Sci. USA *107*, 4820–4824.
3. Hedrick, T.L., Cheng, B., and Deng, X. (2009). Wingbeat time and the scaling of passive rotational damping in flapping flight. Science *324*, 252–255.
4. Norberg, U.M., and Rayner, J.M.V. (1987). Ecological morphology and flight in bats (Mammalia; Chiroptera): wing adaptations, flight performance, foraging strategy and echolocation. Philos. Trans. R. Soc. B Biol. Sci. *316*, 335–427.
5. Ramezani, A., Chung, S.J., and Hutchinson, S. (2017). A biomimetic robotic platform to study flight specializations of bats. Sci. Robot. *2*, eaal2505.
6. Ristroph, L., Ristroph, G., Morozova, S., Bergou, A.J., Chang, S., Guckenheimer, J., Wang, Z.J., and Cohen, I. (2013). Active and passive stabilization of body pitch in insect flight. J. R. Soc. Interface *10*, 20130237.
7. Vance, J.T., Faruque, I., and Humbert, J.S. (2013). Kinematic strategies for mitigating gust perturbations in insects. Bioinspir. Biomim. *8*, 016004.

8. Crall, J.D., Chang, J.J., Oppenheimer, R.L., and Combes, S.A. (2017). Foraging in an unsteady world: bumblebee flight performance in field-realistic turbulence. Interface Focus *7*, 20160086.
9. Ortega-Jimenez, V.M., Greeter, J.S.M., Mittal, R., and Hedrick, T.L. (2013). Hawkmoth flight stability in turbulent vortex streets. J. Exp. Biol. *216*, 4567–4579.
10. Ortega-Jimenez, V.M., Mittal, R., and Hedrick, T.L. (2014). Hawkmoth flight performance in tornado-like whirlwind vortices. Bioinspir. Biomim. *9*, 025003.
11. Bergou, A.J., Swartz, S.M., Vejdani, H., Riskin, D.K., Reimnitz, L., Taubin, G., and Breuer, K.S. (2015). Falling with style: bats perform complex aerial rotations by adjusting wing inertia. PLoS Biol. *13*, e1002297.
12. Boerma, D.B., Breuer, K.S., Treskatis, T.L., and Swartz, S.M. (2019). Wings as inertial appendages: how bats recover from aerial stumbles. J. Exp. Biol. *222*, 204024.
13. Tobalske, B.W., Warrick, D.R., Clark, C.J., Powers, D.R., Hedrick, T.L., Hyder, G.A., and Biewener, A.A. (2007). Three-dimensional kinematics of hummingbird flight. J. Exp. Biol. *210*, 2368–2382.
14. Tobalske, B.W., Biewener, A.A., Warrick, D.R., Hedrick, T.L., and Powers, D.R. (2010). Effects of flight speed upon muscle activity in hummingbirds. J. Exp. Biol. *213*, 2515–2523.
15. Altshuler, D.L., Welch, K.C., Jr., Cho, B.H., Welch, D.B., Lin, A.F., Dickson, W.B., and Dickinson, M.H. (2010). Neuromuscular control of wingbeat kinematics in Anna's hummingbirds (Calypte anna). J. Exp. Biol. *213*, 2507–2514.
16. Ortega-Jimenez, V.M., Sapir, N., Wolf, M., Variano, E.A., and Dudley, R. (2014). Into turbulent air: size-dependent effects of von Kármán vortex streets on hummingbird flight kinematics and energetics. Proc. Biol. Sci. *281*, 20140180.
17. Ravi, S., Crall, J.D., McNeilly, L., Gagliardi, S.F., Biewener, A.A., and Combes, S.A. (2015). Hummingbird flight stability and control in freestream turbulent winds. J. Exp. Biol. *218*, 1444–1452.
18. Biewener, A.A. (2011). Muscle function in avian flight: achieving power and control. Philos. Trans. R. Soc. B Biol. Sci. *366*, 1496–1506.
19. Balint, C.N., and Dickinson, M.H. (2001). The correlation between wing kinematics and steering muscle activity in the blowfly Calliphora vicina. J. Exp. Biol. *204*, 4213–4226.
20. Sato, H., Vo Doan, T.T., Kolev, S., Huynh, N.A., Zhang, C., Massey, T.L., van Kleef, J., Ikeda, K., Abbeel, P., and Maharbiz, M.M. (2015). Deciphering the role of a coleopteran steering muscle via free flight stimulation. Curr. Biol. *25*, 798–803.
21. Fernández, M.J., Springthorpe, D., and Hedrick, T.L. (2012). Neuromuscular and biomechanical compensation for wing asymmetry in insect hovering flight. J. Exp. Biol. *215*, 3631–3638.
22. Vance, J.T., Altshuler, D.L., Dickson, W.B., Dickinson, M.H., and Roberts, S.P. (2014). Hovering flight in the honeybee Apis mellifera: kinematic mechanisms for varying aerodynamic forces. Physiol. Biochem. Zool. *87*, 870–881.
23. Mahalingam, S., and Welch, K.C., Jr. (2013). Neuromuscular control of hovering wingbeat kinematics in response to distinct flight challenges in the ruby-throated hummingbird, Archilochus colubris. J. Exp. Biol. *216*, 4161–4171.
24. Konow, N., Cheney, J.A., Roberts, T.J., Iriarte-Díaz, J., Breuer, K.S., Waldman, J.R.S., and Swartz, S.M. (2017). Speed-dependent modulation of wing muscle recruitment intensity and kinematics in two bat species. J. Exp. Biol. *220*, 1820–1829.
25. Song, J., Luo, H., and Hedrick, T.L. (2014). Three-dimensional flow and lift characteristics of a hovering ruby-throated hummingbird. J. R. Soc. Interface *11*, 20140541.
26. Reynolds, K.V., Thomas, A.L.R., and Taylor, G.K. (2014). Wing tucks are a response to atmospheric turbulence in the soaring flight of the steppe eagle *Aquila nipalensis*. J. R. Soc. Interface *11*, 20140645.
27. Cheng, B., Deng, X., and Hedrick, T.L. (2011). The mechanics and control of pitching manoeuvres in a freely flying hawkmoth (Manduca sexta). J. Exp. Biol. *214*, 4092–4106.
28. Cheng, B., Tobalske, B.W., Powers, D.R., Hedrick, T.L., Wethington, S.M., Chiu, G.T.C., and Deng, X. (2016). Flight mechanics and control of escape manoeuvres in hummingbirds. I. Flight kinematics. J. Exp. Biol. *219*, 3518–3531.
29. Combes, S.A., and Dudley, R. (2009). Turbulence-driven instabilities limit insect flight performance. Proc. Natl. Acad. Sci. USA *106*, 9105–9108.
30. Altshuler, D.L., Quicazán-Rubio, E.M., Segre, P.S., and Middleton, K.M. (2012). Wingbeat kinematics and motor control of yaw turns in Anna's hummingbirds (Calypte anna). J. Exp. Biol. *215*, 4070–4084.
31. Hedrick, T.L., Usherwood, J.R., and Biewener, A.A. (2007). Low speed maneuvering flight of the rose-breasted cockatoo (Eolophus roseicapillus). II. Inertial and aerodynamic reorientation. J. Exp. Biol. *210*, 1912–1924.
32. Cheng, B., Tobalske, B.W., Powers, D.R., Hedrick, T.L., Wethington, S.M., Chiu, G.T.C., and Deng, X. (2016). Flight mechanics and control of escape manoeuvres in hummingbirds. I. Flight kinematics. J. Exp. Biol. *219*, 3518–3531.
33. Mahalingam, S., and Welch, K.C., Jr. (2013). Neuromuscular control of hovering wingbeat kinematics in response to distinct flight challenges in the ruby-throated hummingbird, Archilochus colubris. J. Exp. Biol. *216*, 4161–4171.
34. Sane, S.P., and Dickinson, M.H. (2001). The control of flight force by a flapping wing: lift and drag production. J. Exp. Biol. *204*, 2607–2626.
35. Zusi, R.L., and Bentz, G.D. (1984). Myology of the purple-throated Carib (Eulampis jugularis) and other hummingbirds (Aves: Trochilidae). Smith. Contrib. Zool. 1–70.
36. Dellow, P.G., and Lund, J.P. (1971). Evidence for central timing of rhythmical mastication. J. Physiol. *215*, 1–13.
37. Alfaro, M.E., and Herrel, A. (2001). Introduction: major issues of feeding motor control in vertebrates. Am. Zool. *41*, 1243–1247.
38. Konow, N., and Sanford, C.P.J. (2008). Is a convergently derived muscle-activity pattern driving novel raking behaviours in teleost fishes? J. Exp. Biol. *211*, 989–999.
39. Katz, P.S. (2016). Evolution of central pattern generators and rhythmic behaviours. Philos. Trans. R. Soc. B Biol. Sci. *371*, 20150057.
40. Liao, J.C. (2007). A review of fish swimming mechanics and behaviour in altered flows. Philos. Trans. R. Soc. Lond. B Biol. Sci. *362*, 1973–1993.
41. Altshuler, D.L., Bahlman, J.W., Dakin, R., Gaede, A.H., Goller, B., Lentink, D., Segre, P.S., and Skandalis, D.A. (2015). The biophysics of bird flight: functional relationships integrate aerodynamics, morphology, kinematics, muscles, and sensors. Can. J. Zool. *93*, 961–975.
42. Maeda, M. (2014). Aerodynamics of flapping flight interacting with environments. https://core.ac.uk/download/pdf/97062894.pdf.
43. Basmajian, J.V., and Stecko, G. (1962). A new bipolar electrode for electromyography. J. Appl. Phys *17*.
44. Ravi, S., Crall, J.D., Fisher, A., and Combes, S.A. (2013). Rolling with the flow: bumblebees flying in unsteady wakes. J. Exp. Biol. *216*, 4299–4309.
45. Park, H.J. (2006). Three Component Velocity Measurements in the Tip Vortex of a Micro-Air-Vehicle (Air Force Institute of Technology).
46. Hedrick, T.L. (2008). Software techniques for two- and three-dimensional kinematic measurements of biological and biomimetic systems. Bioinspir. Biomim. *3*, 034001.
47. Maeda, M., Nakata, T., Kitamura, I., Tanaka, H., and Liu, H. (2017). Quantifying the dynamic wing morphing of hovering hummingbird. R. Soc. Open Sci. *4*, 170307.
48. Zar, J.H. (2010). Biostatistical Analysis, Fifth Edition (Prentice Hall).
49. Liu, H. (2009). Integrated modeling of insect flight: from morphology, kinematics to aerodynamics. J. Comp. Phys. *228*, 439–459.

STAR★METHODS

KEY RESOURCES TABLE

REAGENT or RESOURCE	SOURCE	IDENTIFIER
Biological Samples		
Archilochus colubris	Wild caught at Concord Field Station	Wild caught at Concord Field Station Data presented in Table S2
Experimental Models: Organisms/Strains		
Archilochus colubris	Wild caught at Concord Field Station	Wild caught at Concord Field Station Data presented in Table S2
Instrumentation		
Highspeed camera	Photron FASTCAM SA3	http://www.highspeedimaging.com/photron-fastcam-sa3/
Amplifiers	Grass Technologies, Warwick RI	https://neuro.natus.com/
A/D converter	Powerlab 8/30	https://www.adinstruments.com/content/30-series-430-830-1630
Hot-wire anemometer	55P91 probe, Dantec Dynamics, Denmark	https://www.dantecdynamics.com/products-and-services/triple-sensor-gold-plated-wire-probe
Micro connectors	Digikey model 455-2196-1-ND	https://www.digikey.com/product-detail/en/jst-sales-america-inc/SACHP-003G-P0.2/455-2196-1-ND/1647793
Electromyography wire	California Fine wire, Grover Beach Ca. Polyethylene-coated stainless steel, Bi-filar 0.05 mm diameter	from California Fine Wire: http://www.calfinewire.com/
Software and Algorithms		
MATLAB R2017a	MATLAB (2017). version 9.2.0 (R2017a), The MathWorks, Natick, Massachusetts	http://www.mathworks.com/
CFD solver	[42]	N/A

LEAD CONTACT AND MATERIALS AVAILABILITY

Further information and requests for resources and data should be directed to and will be fulfilled by the Lead Contact, Nicolai Konow (nicolai_konow@uml.edu).

This study did not generate new unique reagents.

EXPERIMENTAL MODEL AND SUBJECT DETAILS

Four Ruby-throated hummingbirds (*Archilochus colubris*) were caught at the Concord Field Station in Bedford, MA and housed in 0.5 × 0.5 × 0.5 m chambers for one week of acclimation, with fortified nectar solution (Nektar Plus, Nekton USA) provided *ad libitum* from a hummingbird feeder. Experiments were conducted in accordance with a Harvard University Institutional Animal Care and Use protocol. Morphological measurements of specimen presented in ST2.

METHOD DETAILS

Electrode implantation for electromyography

Twisted fine-wire electrodes with offset bipolar tips [43] were made from gold- covered silver wire (California fine wire, 0.1 mm ⌀). For birds 1 and 2, the electrode pole spacing was 1 mm and the poles were 0.5 mm long. To further limit cross-talk between electrodes in the two muscles, we decreased pole length to 0.25 mm and spacing to 0.5 mm for birds 3 and 4. The 600 mm long EMG wires were crimped and soldered into micro-connectors (Digikey model 455-2196-1-ND) for connection to amplifiers during experiments.

Electrodes were implanted into the pectoralis and supracoracoideus muscles using a 25G hypodermic needle with the birds in a light plane of isoflurane anesthesia (1%–1.5% via mask), after cleaning the implantation sites with isopropyl alcohol. We minimized cross-talk by inserting the electrode recording poles as far apart as possible given the proximity and small size of the muscles of interest. A standardized approach was used to implant electrodes, as follows. For the pectoralis muscle, the hypodermic needle

was guided rostro-dorsally, so that the electrode recorded from the mid-sternobranchialis region. For the supracoracoideus muscle, the hypodermic needle was guided caudo-dorsally along the sternal keel with the bevel medially oriented until it touched the sternum. The electrode wires were glued to caudoventral plumage using cyanoacrylate glue. Following implantation, the birds were administered a meal of Nectar Plus and then allowed to recover for a period ranging from two hours to overnight in a dark room with *ad libitum* nectar. After experiments, the electrodes were removed under light anesthesia. Electrodes were implanted on only one side of each bird (right side in birds 1 and 2, left side in birds 3 and 4). However, by rotating the vortex generator to different positions we could alter the flow conditions and thus measure neuromuscular activity when the implanted wing was immersed in upwash as well as downwash.

Flight tests

Flight tests were conducted in the same wind tunnel used in [17, 44] that measured 6-m long and was suction-type, open-return wind tunnel with a 1.5 L x 0.5 W x 0.5 H m test section. An intermediate cruising speed of 5 m/s was used for the experiments [13]. Each subject was released into the test section, which contained a longitudinal-vortex generator near the inlet as well as a downstream perch. The vortex generator was a vertically oriented symmetric NACA0015 wing with 25-cm span and 10-cm chord (Figure 1). A syringe was used to dispense sucrose solution through a polyethylene tube to its aperture at the wingtip, to attract birds to feed while flying in an appropriate position relative to the vortex generator. All birds began feeding within five minutes of being released into the test section. During flight trials, kinematics of the wings, tail, and body were recorded at 1000 Hz using three phase-locked Photron SA3 high-speed cameras (Figure 1).

During experiments, EMG signals were amplified (1000x) and filtered (60Hz notch, 30-3000Hz band-pass; p511-G amplifiers Grass Technologies, Warwick RI). The minimally processed signals were A/D converted at 10 kHz to hard drive via a Powerlab 8/30 (ADinstruments). The camera trigger pulse was also A/D converted to synchronize EMG and kinematic data. The EMG signals were processed and spikes were isolated from the time-history for further analysis using methods as described in [15].

QUANTIFICATION AND STATISTICAL ANALYSIS

Flow Conditions

Airflows were quantified using a three component hot-wire anemometer (55P91 probe, Dantec Dynamics, Denmark) sampling at 1kHz, and calibrated against a standard pitot-static tube (Figure S1). The symmetrical nature of the vortex generator results in nominally laminar flow when it was aligned with the free-stream (0°), or a quasi-steady vortex with anti-clockwise (−15° rotation) or clockwise (15° rotation) flow downstream of the wing tip. Orientation of the vortex generator at 0° with respect to the free stream caused a flat velocity profile across the test section, with a small velocity deficit caused by the drag of the vortex generator (Figures 1A, 1B, and S1). Rotating the vortex generator ± 15° caused a steady longitudinal vortex in the wake with clockwise and anticlockwise polarity respectively, due to the pressure difference over the top and bottom surfaces of the vortex generator (Figures 1C, 1D, and S1). Time-resolved velocity measurements did not vary significantly within the vortex (Figure S1) and a steady velocity was present across the vortex (Figure S1). As expected, the mean perturbation velocity was nearly zero at the vortex core while we measured a maximum of nearly 4 m/s of upwash and downwash velocity on either side of the core (Figure S1). The upwash and downwash monotonically decreased with increasing lateral distance from the core and the size of the vortex of nominally equivalent to the wingspan of the birds (compare Figure S1 to Table S1). The increased frontal area of the upstream vortex generator, when it was rotation by 15°, caused a velocity deficit in the wake resulting in the longitudinal flow speed to be slightly lower. The velocity profile within the vortex closely matched theoretical predictions and prior wing-tip vortex measurements [45]. The feeder was aligned with the core of the vortex (Figure 1A) to ensure symmetry of the perturbation; hence, a hummingbird flying within the vortex experienced an aerodynamically induced rotation (Video S1), with one wing immersed in upwash (vertical flow oriented upward) and the other wing in downwash (vertical flow oriented downward). Each bird was flown under all three orientations of the vortex generator, and the order of trials was randomized within individuals.

Reconstruction of kinematics

Marker points, consisting of non-toxic water-soluble white paint, in recorded flight sequences were digitized using an open-source MATLAB-based routine [46]. A static calibration cube that filled the volume of interest in the test section was used for spatial calibration via direct linear transformation [46]. Markers over the shoulder joints (where the wings attach to the thorax), the positions of the wrists along the leading edges, the tips of the 5th primary feathers along the trailing edges, the base of the tail (midline of where the tail meets the body in the sagittal plane), and the tips of the most lateral tail feathers were digitized (see Figure 1), for a total of nine points digitized over 0.5 s of flight (20-22 wingbeats) for each trial. Subsequent kinematic analyses were performed in MATLAB. Digitization error in point localization was much smaller than the mean pairwise marker distances (~60 pixels). This error is expected to be manifest only at higher frequencies, on the order of the Nyquist frequency. To remove any higher frequency fluctuations due to digitization error, position data were filtered using a 4th order, low-pass Butterworth filter with a cutoff frequency of 200 Hz, which is lower than the Nyquist frequency (500 Hz) but higher than the flapping frequency (~45 Hz).

Wingbeat kinematics were derived from the digitized positions of the shoulder joints, the leading edge, and the trailing edge of each wing using the coordinate system shown in Figure 2A. For each stroke, the flapping frequency was calculated as the inverse of the wing beat period, independently measured for the left and right wings. Stroke plane angle (χ) was calculated in the global coordinate

system for each wingbeat by estimating the pitch angle of a 2D regression line of the position of the leading edge throughout a stroke projected onto the x-z plane (Figure 2A). Wing position angle (ϕ) was measured as the angle of the leading edge (relative to 0 degrees, when wings are held straight out to each side) along the stroke plane through time, and stroke amplitude was the total angle swept between the top of the upstroke and bottom of the downstroke (i.e., $\phi_{max} - \phi_{min}$). Wing elevation (θ) was measured as the perpendicular angle between the leading edge and the stroke plane. Wing rotation (α) was measured with respect to the stroke plane as the angle formed between the wing plane and the ordinate axis of the stroke plane. The angle of attack was estimated at 0.75 of the span using the coordinate system described in [47] by taking into account the angular velocity of the wing at that position, rotation and the mean velocity of wind. For angle of attack estimation in laminar flow the wind velocity (as shown in Figure S1) was aligned with the wind tunnel longitudinal axis at all wing positions in the stroke, Figure S3. For flight in the vortex condition, rotational symmetry of the vortex was assumed and the wind velocity at each stroke position was inferred from the azimuthal position of the wing. Body orientation of the birds was measured in the global coordinate system by creating a plane using the digitized shoulder points and the tail base in the sagittal plane similar to that described in [17]. Fan angle of the tail was calculated as the angle between the vectors connecting the lateral tail tips to the tail base. The body orientation and tail fan angle was measured for the entire flight sequence and mean values were compared across the different free-stream treatments.

Data analysis and statistical tests

The dataset for analysis consisted of 7 wingbeats per subject (4) and flow condition (3) for a total of 84 wingbeats. Wing kinematics of subjects were pooled depending on the flow condition (i.e., laminar flow, immersed in vortex upwash, or immersed in vortex downwash), experienced by the implanted wing Figure 1. Mean and standard deviation of the pooled kinematics of all birds for each flow condition was then calculated. The mean angles of body yaw and tail fanning were compared across factorial pairs of flow conditions using repeated-measures ANOVA.

The timing of each muscle's activity (on- and offset) was measured to compare activation profiles across flow conditions. Muscle recruitment was evaluated based on peak recruitment intensity (mV) and integrated area (iEMG; area under rectified EMG, V · s). For each muscle, EMG measurements were compared across flow conditions. Statistical analyses of EMG measurements involved mixed model ANOVAs with flow condition as a fixed effect, factoring individual as well as the interaction term between individual and flow condition as independent effects [48]. All statistical calculations were performed in MATLAB.

Computational fluid dynamics analysis

Computational fluid dynamics analysis was conducted using an in-house solver based on a fortified Navier-Stokes solver [49]. A general formulation of the multi-blocked, overset grid, fortified solutions to the Navier-Stokes equations was performed in the global system (X, Y, Z) (Figure S2). The governing equations were the three-dimensional, incompressible, unsteady Navier-Stokes equations written in strong conservation form for mass and momentum. When the equations were solved for each block, the aerodynamic forces $F_{aero} = (F_{ax}, F_{ay}, F_{az})$ exerted on the body and wings were evaluated by a sum of aerodynamic forces in the global coordinate system. The simulations in this study were conducted using a previously developed, detailed morphological model of a hummingbird assuming rigid body and wing structure [42, 47]. The wing length and mean chord length were 69.3 and 19.5 mm, respectively. The wing shape and size used for numerical simulations were similar to the species used for experiments. The simulations parameters including grid sizing and sensitivity were similar to those used in [42].

Wing kinematics in smooth and vortex flow were constructed based on *in vivo* measurements in each condition. To derive kinematic variables for the model, we calculated the mean wingbeat cycle with respect to the stroke plane angle (Figures 2C–2E), and reconstructed mean kinematics mathematically using a third-order Fourier series, as in [49].

To assess the effect of the perturbation on a hummingbird flying with bilaterally symmetric kinematics, CFD simulations were performed where the vortex generator was oriented at 15° upstream and the hummingbird flying with the kinematics measured in laminar flow conditions. While the overall trend of the velocities within the longitudinal vortex in CFD simulation matched the experiments, the velocity magnitudes were significantly higher in the latter, see Figure S4. Due to the large disparity in the longitudinal vortex between simulation and experiments, all remaining CFD simulations were conducted assuming laminar inflow conditions. We hypothesized that implementing the asymmetric wing kinematics measured from hummingbirds flying in the longitudinal vortex in a simulation assuming laminar inflow would result in the modeled hummingbird producing asymmetric lift and a roll torque in the opposite direction from that imposed by the longitudinal vortex in the experiment.

In our parametric study, we simulated the flight of birds with four different wing kinematic profiles. Simulation cases 1 and 2 employed wing kinematics that matched those observed in the laminar inflow and clockwise vorticity conditions, respectively (both simulated in laminar flow, as stated above). Although there were slight angular differences between the right and left wings in laminar flow, we adopted the average wing kinematics for all cases (Figures 2C–2E). Cases 1 & 2 were considered to be baselines for validating the simulation, by determining whether total vertical force produced would be sufficient to support the bird's weight in laminar flow (Case 1), and by validating the hypothesis that the asymmetric kinematics observed in vortex flow would result in a counterclockwise torque being produced by the bird (Case 2). To determine the salient components of the asymmetric kinematics observed in birds flying in the longitudinal vortex, two additional parametric systems were created that consisted of hybrids between the kinematics observed in birds flying laminar and vortex flows. For Case 3, the kinematic hybrid combined wing elevation angles taken from the clockwise vortex condition with all other kinematic parameters (including wing rotation angles and position) from laminar flow. Case 4 incorporated wing rotation angles from the clockwise vortex condition and all other parameters (including wing elevation

and position) from the laminar flow condition. We simulated five wingbeat cycles of flight in each case, and calculated the mean vertical force and roll torque produced.

DATA AND CODE AVAILABILITY

The raw datasets and high speed videos have not been uploaded in a public repository .They can be provided upon request to the Lead Contact.